Parallel Multiclass Support Vector Interpretation of Haemodynamic Parameters for Manifestation of Aortic and Arterial Occlusive Diseases

S.H. Karamchandani[1], V.K. Madan[2], P.M.Kelkar[3], S.N. Merchant[1], U.B. Desai[4]
[1]Indian Institute of Technology – Bombay, Mumbai 400076, India.
[2] Kalasalingam University, Krishnankoil, Virudhunagar Dt (TN) 626126, India.
[3]Sneha Health Care Centre, Mumbai 400602, India.
[4]Indian Institute of Technology – Hyderabad, Hyderabad, India.
{sunilk, merchant}@ee.iitb.ac.in, KLvkmadan@gmail.com, drprasannakelkar@yahoo.com, ubdesai@iith.ac.in.

Abstract

Aortic and arterial occlusive diseases are congenital conditions manifested in impedance plethysmography and are difficult to interpret. A parallel multiclass support vector classification of haemodynamic parameters computed from plethysmographic observations is proposed for diagnosis of aortoarteritis, atherosclerotic narrowing and coarctation of aorta. The proposed support vector algorithm was able to detect more precisely the presence of thrombotic occlusions at proximal and distal arteries. The proposed method provided better accuracy and sensitivity of 97.46% and 98.3% compared to principal component analysis (PCA) based backpropagation and non-weighted support vector architectures respectively. The results of the genotype were ably supported by receiver operating characteristics (ROC) curves which depict a ratio of true positive rate and false positive rate of over 0.9 for all classes as compared with ratios varying from 0.7 to 0.9 for majority of classes as observed in case of non weighted architecture. A reduction of over 60% in negative likelihood ratio with a 5% increase in negative predictive value was observed as compared to Elman and PCA based backpropagation architectures. The results were validated from angiographic findings at Grant Medical College, J.J. Hospital, and Bhabha Atomic Research Centre all in Mumbai. The proposed method also distinguished cases with nephritic syndrome, lymphangitis, and venous disorders against those with arterial occlusive diseases. Application of the proposed method has potential to enhance performance of impedance plethysmography.

Keywords: Impedance Cardiovasography, Aortic Occlusive Diseases, Arterial Occlusive Diseases, Parallel Multiclass support vector machines.

I.   Introduction

Vascular obstruction to blood flow at young age are very low (~0.01%). However they become significant above 40 years of age (~1%) and above 60 years of age (~20 to 30%) [1]. Different non invasive techniques such as photo plethysmography and Doppler exist for tracking vascular obstructions. The photo plethysmography is useful on fingers, toes and ear lobes, but not on limbs [2]. The conventional Doppler is useful for superficial blood vessels, and the performance is and operator dependent. The color Doppler is an expensive technique and demands expertise. Moreover its performance degrades significantly for collateral circulation and distal runoff. Impedance cardiovasography (ICVG) based on the principle of impedance plethysmography is a non invasive procedure for diagnosis of aortic occlusive diseases such as coarctation of aorta, aortoarteritis, atherosclerotic narrowing and Leriche's syndrome [3-4]. Calin et al. have designed an equilibrated bridge which uses an external signal generator for measuring haemodynamic parameters on the plethysmographic wave [5]. However the procedure discussed for normal subjects does not portray the variations in the plethysmographic waves for diseased cases [6]. A color relation analyzer (CRA) classifier detects plethysmographic signals for lower limb peripheral vascular occlusive disease (PVOD) assessment [7], and signals are measured at the toes to arrive at disease prognosis. It does not provide analysis of haemodynamic parameters. Hull et al restrict the use of impedance plethysmography for detection of deep vein thrombosis [8]. Forearm impedance plethysmography introduced for monitoring the cardiac pumping function [9] was not useful for determining absolute stroke volume.

It is proposed to enhance diagnostic capabilities of impedance plethysmography through measurement of hemodynamic parameters of amplitude and time for diagnosis of occlusive diseases such as aortoarteritis, atherosclerotic narrowing and coarctation of aorta. For the study of peripheral circulation, impedance cardiograph was recorded from the neck, and at four locations in the lower extremities of thigh, knee, calf and ankle using ICVG [10]. The mentioned measurements were used as pattern recognition parameters and a real time technique classifier was developed using an assortment of multiclass parallel support vector machine (pSVM) algorithms.

1

The paper describes below the acquisition of the plethysmographic data, estimation of the haemodynamic parameters and their relevant significance, interpretation of the parameters for diagnosis of aortic and arterial occlusive diseases, the proposed multiclass pSVM, experimental results, conclusion, and a possible direction for further work.

II.   Data Acquisition

Impedance plethysmography gives an indirect assessment of blood volume changes in any part of the body segment as a function of time [11-14]. The impedance plethysmography relates volume of blood (ΔV) entering a body segment during entire systole to the total change in impedance (ΔZ) occurring during the period [15] as

$$\Delta V = \rho_b \frac{L^2}{z_0^2} \Delta Z \tag{1}$$

where ρ_b is the resistivity of blood, L is the length of the limb segment, and z_o is the basal impedance of the body segment. This change in impedance is measured for locations of thigh, knee, calf and ankle in the supine and elevated postures (45°).

About 200 subjects with severe joint pains, oedema in legs, pain in calf muscles, and swelling in the ankle were subjected to plethysmographic observations for disease characterization. ECG electrodes, E1 and E2 were applied in the lead II configuration. The sensing electrodes were applied around the segment of interest with the patient in the supine, while current electrodes were applied as far away as possible from sensing electrodes on the limb. The magnitude of current flowing through the body was 2 mA. The waveforms were recorded from each of the extremity for about 300 sec followed by ensemble averaging to enhance signal to noise ratio. A typical impedance waveform is shown in Figure 1(e).
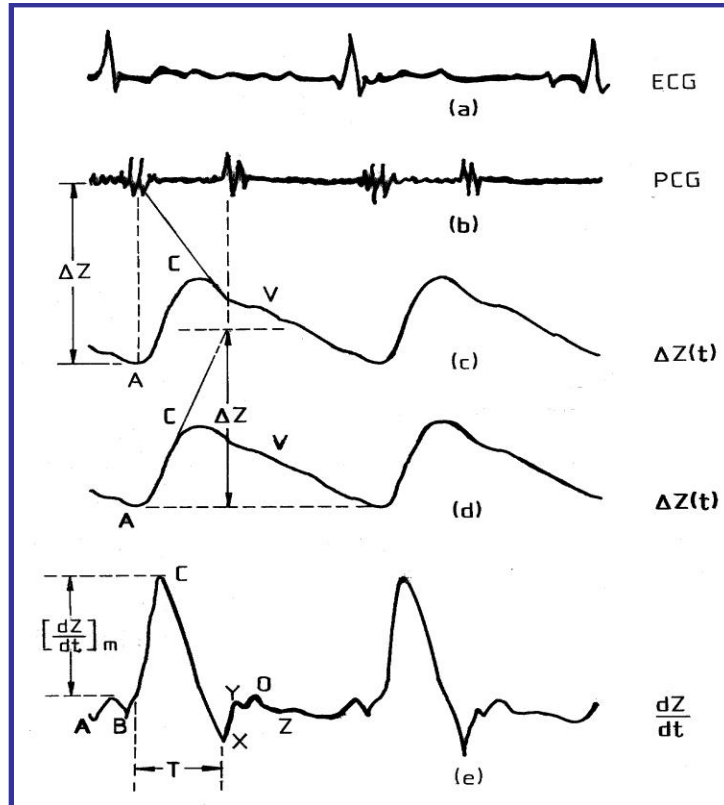

Fig.1: Impedance Cardiovasographic ΔZ (t) and dZ/dt waveforms in relation to electrocardiogram and phonocardiogram
(Courtesy: *Electronics Division, BARC*)

Haemodynamic parameters used were z_o, ΔZ (t), dZ/dt, and the time elapsed between the R-wave and various phase reversal points in the impedance waveform [16]. An ICVG system provides normalized rate of change of impedance (NdZ/dt) [17-18].

III.   Computation of Haemodynamic Parameters from Impedance Waveform

Parametric measurements of amplitude and time are useful for computing haemodynamic parameters from the impedance waveform. The maximum rate of change of impedance is calculated as a measure of the peripheral blood flow while the relative time measurements are performed in terms of differential pulse arrival time (DPAT).

A.   Peripheral Blood Flow

Change in impedance, ΔZ, is obtained as the product of the maximum rate of change of impedance with systolic time interval T_s. Modifying Eq. 1, we get,

$$dV = \rho_b \frac{L^2}{Z_O{}^2} (dZ/dt)_m T_s \qquad (2)$$

where $(dZ/dt)_m$ is the maximum amplitude of the normalized impedance waveform
Resistivity is related to other parameters as

$$\rho_b L^2 = Z_o V \qquad (3)$$

From (2) and (3)

$$dV = V \frac{(dZ/dt)_m T_s}{z_o} \qquad (4)$$

Blood Flow in ml per 1000 cc of body tissue per cardiac cycle is defined as

$$dV = 1000 \frac{(\frac{dZ}{dt})_m}{z_o} T_s \qquad (5)$$

The product $(dZ/dt)_m T_s$ represents the total change in the impedance during the systolic period. BCX in Fig. 2(b) depicts systolic wave, and T_s was computed by measuring the distance RX-RB in the figure. T_s represents the left ventricular ejection time (LVET) and it remains fairly constant in a person [19]. Maximum amplitude of dZ/dt waveform was computed by measuring BC. The Eq 5 is rewritten as

$$dV = 1000 \frac{(BC)}{z_o} (RX - RB) \qquad (6)$$

The normalized dZ/dt waveform measures the ratio $(BC)/z_o$. From Eq. 6 we get parameter Blood Flow Index (BFI) representing maximum amplitude of $\frac{dZ}{dt}$ for arterial blood flow.

$$\text{Blood flow Index} = k \frac{(BC)}{z_o} \qquad (7)$$

B.   Differential Pulse Arrival Time

As shown in Fig. 2, RC represents the time taken by the blood to reach a particular location measured with respect to the R-wave of the ECG, and is designated as pulse arrival time (PAT). Differential pulse arrival time (DPAT) between two locations was obtained from PAT by subtracting RC of proximal location from RC of distal location.

Table 2: Ideal DPAT conditions at measured anatomical locations

Segment	DPAT (ms)
Neck to upper arm	30 ± 2.5
Upper arm to elbow	20 ± 2.5
Elbow to wrist	25 ± 2.5
Neck to upper thigh	75 ± 5.0
Upper thigh to knee	35 ± 5.0
Knee to ankle	40 ± 5.0

Data from Clinical Investigation on Normal Subjects at J.J.Hospital, Mumbai
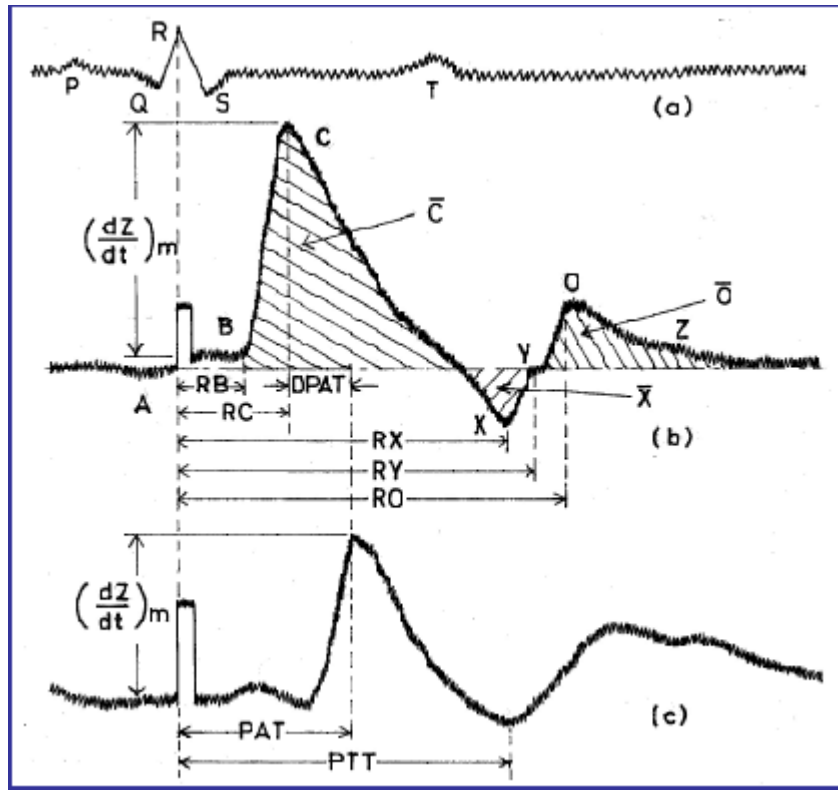
Fig. 2. Impedance waveforms at proximal and distal locations.
A: Atrial Systole; B: Aortic valve opening; C: Instant of Maximum Ejection Rate of Left Ventricle; X: Aortic valve closure; Y: Pulmonary valve closure; O: Mitral Valve Opening; Z: End of Rapid Filling Phase.
(Courtesy: *Electronics Division, BARC*)

It is observed from the Table 2 that the DPAT may increase, remain unchanged or decrease depending upon whether the occlusion is complete, partial or has generalized narrowing of the blood vessels. Protective role of collaterals on myocardial electrophysiology was suggested in [20-21]. In case of complete occlusion, blood reaches the distal segment through the collaterals developed biologically and therefore traverses more distance taking more time to reach the distal segment, and hence causing an increase in the value of DPAT. In case of partial occlusion, change in the value of DPAT may not be significant. In case of generalized narrowing of blood vessels the blood may reach the distal segment faster as the blood velocity increases due to decreased lumen of blood vessel and its compliance. This causes a decrease in the value of DPAT.
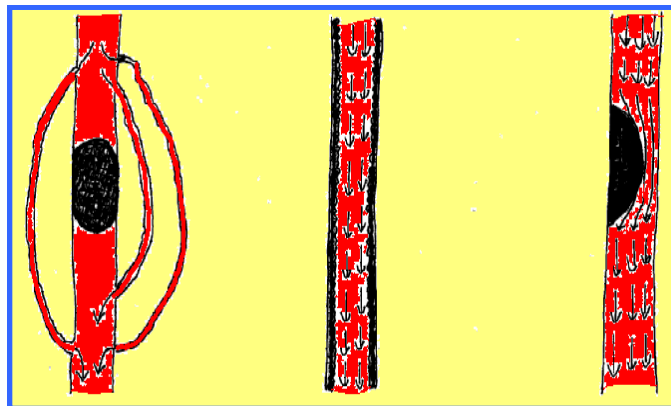

Figure 3: (a) Complete Occlusion (b) Generalized Narrowing of the Arteries (c) Partial Occlusion

IV. Interpretation of haemodynamic parameters in diagnosis of Aortic and Arterial Occlusive Diseases

From the ICVG waveforms, the parameters BFI and DPAT are extracted at four locations; thigh, knee, calf and ankle from both the right and the left limbs. It provides feature vectors for multiclass pSVM for diagnosis and disease characterization.
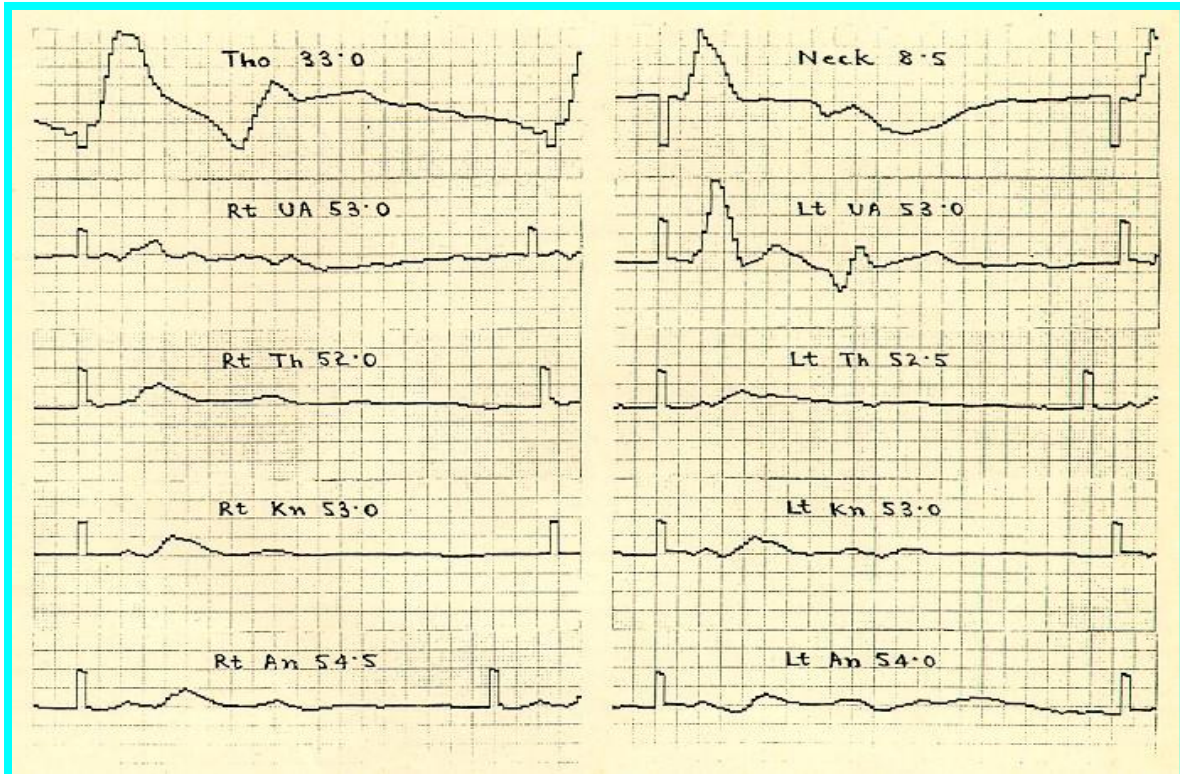

Figure 4: ICVG waveforms recorded from the patient (SC-40-F)

ICVG waveform recorded from patient SC-40-F with aortoarteritis. Polyphasic C wave at thigh level can be observed which is specific to aortoarteritis.

Table 3: Parameters extracted from subject SC-40-F

Location	Right Leg		Left Leg	
	BFI	DPAT	BFI	DPAT
Upper Arm	0.98	20	0.93	20
Thigh	0.75	60	0.79	40
Knee	0.85	50	0.93	50
Calf	0.66	-	0.82	-
Ankle	0.80	20	0.61	50

Interpretation of the BFI and DPAT for arriving at the exact diagnosis is tabulated in 4.

Table 4: Interpretation of haemodynamic parameters for assessment of physiological functionality

Physiological functionality	Interpretation of Haemodynamic Parameters
Aorto Arteritis	Decreased BFI with marginal increase in DPAT in both legs. Systolic wave at the thigh level, which is caused by either multiple occlusions or narrowing in the aorta.
Atherosclerotic narrowing of the aorta	Significant decrease in the value of DPAT at thigh level in both the extremities with marginal decrease in the value of BFI. The morphology of the dZ/dt waveform is different in these cases due to contribution from change in the resistivity of blood moving with higher velocity. These changes are evident at knee and ankle locations due to higher bone to muscle ratio. The amplitude of the systolic wave is either normal or increased in contrast to other conditions and is not representative of the value of blood flow
Occlusions at aorto-iliac bifurcation	Characterized by marked decrease in blood flow at thigh level with a marked increase in DPAT at the knee location. If such changes are observed in one extremity, other remaining normal, such a subject is diagnosed as hemi-Leriche's syndrome.
Co-arctation of the aorta	Blood flow in both the lower extremities at the thigh location is significantly reduced with increase in the value of DPAT.
Nephrotic syndrome, Lymphangitis Deep vein thrombosis	There is a marked decrease in blood flow without any abnormalities in value of DPAT. However oedema due to these diseases causes a marked decrease in the value of basal impedance z_o, which is a clear indication for the clinicians to classify the subject to have oedema of extra vascular nature. The diagnosis of arterial occlusive diseases if present is not possible in such cases by impedance cardiovasography. A case of lymphangitis is reported in Table 5.

ICVG data recorded from a 48 years old male with lymphangitis in the left lower extremity. The amplitude of the waveform does not show any variation on elevation of the limb. Table 5 depicts z_o, observed in the left extremity with lower impedance values.

Table 5: ICVG parameters for subject with lymphangitis

Location	Right Leg			Left Leg		
	BFI	DPAT	z_o	BFI	DPAT	z_o
Thigh	0.88	70	25.51	0.48	70	16.14
Knee (s)	1.41	20	54.21	0.63	20	31.99
Calf (s)	1.64	-	48.73	0.81	-	32.69
Ankle(s)	1.57	20	69.15	0.79	20	27.49
Ankle(e)	1.66	-	71.03	0.89	-	34.44

V. Proposed Architecture of multiclass Parallel Support Vector Machine (pSVM)

Based on the construes in Section IV, a taxonomical classification of the cardiovasographic data into seven different classes was proposed and depicted in Table 6.

Table 6: Classification of the cardiovasographic data

Assigned Class	Anatomical Condition
I	Normal
II	Narrowing
III	Block
IV	Good Collaterals
V	Moderate Collaterals
VI	Poor Collaterals
VII	Further Block

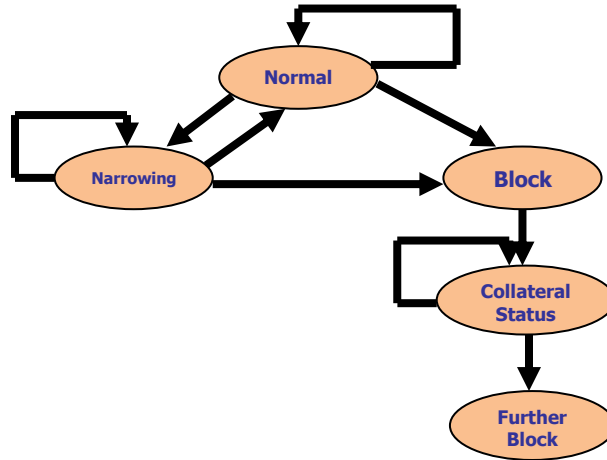The status at each of the considered locations is established according to the flow chart shown in Fig. 5.

Fig. 5. Flow chart for identification of block and status of collateral circulation using extracted BFI and DPAT parameters based on the depicted anatomical conditions

A multiclass pSVM was proposed. It helps in determining location of anatomical block, and in predicting the status of collateral circulation leading to the diagnoses of aortic and arterial occlusive diseases. The pSVM is useful for multiclass classification using either the one versus all (OVA) or one versus one technique (OVO). The performance of OVA classification is quite comparable to OVO method [22-23]. The latter has its lesser training time due to a smaller training data set for each classifier [24]. Due to existence of seven different classes, the multiclass pSVM designed consisted of 7 choose 2, meaning 21 possible combinations, and hence separate SVMs to execute the OVA architecture. As depicted in Fig. 6, SVM 1 learns from outputs of class I and class II, SVM 2 from class I and class III, thus SVM 21 will compare the outputs of class VI and class VII.
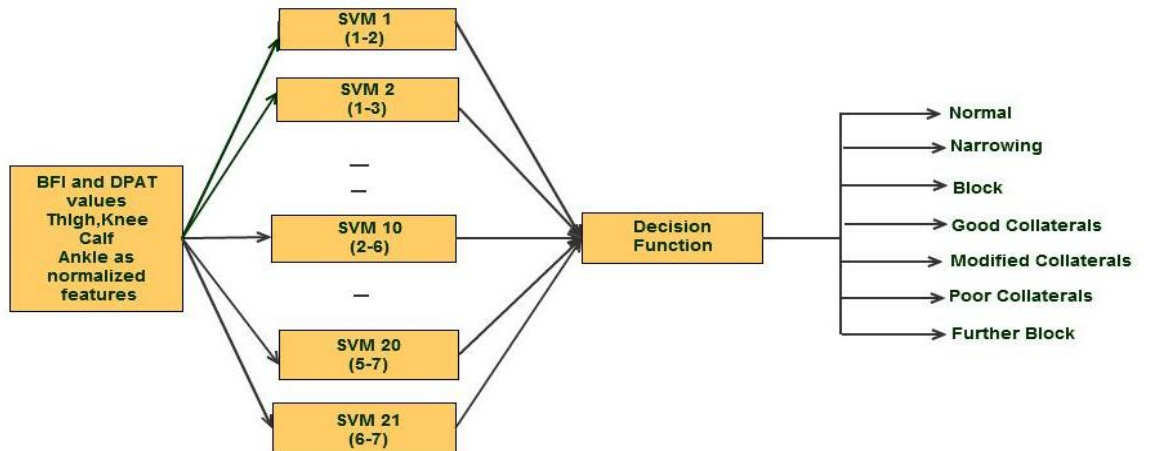

Fig. 6. Proposed pSVM architecture for multiclass classification

The pSVM was implemented in weighted and non weighted architectures. Weighted multiclass SVM assigned a different value of penalty parameter for each training sample thus compensating for the undesirable effects caused by the uneven size of the eight training classes [25]. This is incorporated in the proposed algorithm by applying equal weights to the training sample belonging to same class, and setting weights for different classes with an inverse proportion to the training class size. The weights assigned to the individual classes are given as

$$w(i) = \frac{n - n_i}{n} \qquad (8)$$

where $w(i)$ represents the weight assigned to the ith class, n is the total number of training samples and n_i represents the number of training samples in the ith class. The demographics of the individual seven classes and their calculated weights are shown in Table 7.

Table 7: Demographics of the training classes for pSVM architecture

Classes	I	II	III	IV	V	VI	VII
No of Training set	272	166	92	51	46	32	21
weights for each class	0.6	0.75588	0.8647	0. 925	0.9324	0.9529	0.9691

For the training vectors (x_i, y_i), i = 1, 2, 3…n, each of the twenty one SVMs solve a binary classification problem which is implemented as a soft margin classifier in Eq. 9. $x_i \epsilon \mathbb{R}^n$ represents feature vectors and $y_i \epsilon \{-1, +1\}$ as the complementary outputs of binary classifier.

$$\min_{w^{ij}, b^{ij}, \xi^{ij}} 1/2 \ (w^{ij})^T w^{ij} + C \sum_t \xi_t^{ij}$$

with

$$(w^{ij})^T \phi(x_t) + b^{ij} \geq 1 - \xi_t^{ij} \text{ , if } x_t \text{ in the } i^{th} \text{ class}$$
$$(w^{ij})^T \phi(x_t) + b^{ij} \geq -1 - \xi_t^{ij} \text{ , if } x_t \text{ in the } j^{th} \text{ class}$$
$$\xi_t^{ij} \geq 0 \qquad (9)$$

The feature vectors are mapped to a higher dimension using a radial basis kernel ϕ as implemented in Eq. 10

$$\phi(x_i, x_j) = \exp\left(-\gamma \left\| x_i - x_j \right\|^2\right) \qquad (10)$$

$C > 0$ is a penalty parameter on the training error and ξ_i is a positive slack variable. Keerthi et al [26] indicated that if complete model selection (dynamic changes in C and γ) using the radial basis kernel were conducted, there was no need to consider linear SVM. The sigmoid kernel with scaling parameter 'a' and shifting parameter 'γ' was used as in Eq. 11 where negative values of γ are preferred to control the threshold of mapping in pSVM.

$$\phi(x_i, x_j) = \tanh(ax_i^t x_j + \gamma) \qquad (11)$$

However, the kernel matrix using sigmoid may not be positive definite, has a higher number of parameters than RBF and suggests lower accuracy than RBF [27] kernels. Twenty one hyperplanes were created in the feature space $\emptyset$. The weight $w \epsilon \emptyset$ denotes a dot product space and b represents the shift of the hyper plane in that space. The support vector algorithm was based on maximizing the hyper plane between any two classes of data in a higher dimension feature space $\emptyset$. $C(\sum_{j=1}^{j=l} (\xi_j^i)_t$ term indicates that two data sets are not linearly separable. The optimum values of required parameters, *C* and *γ*, were determined by maximizing the cross validation prediction. Each SVM solved a dual quadratic optimization problem given as

$$\max_{\alpha \in \mathbb{R}^n} W(\alpha) = \sum_{i=1}^n \alpha_i - \frac{1}{2} \sum_{i=1}^n \sum_{j=1}^n \alpha_i \alpha_j y_i y_j \phi(x_i, x_j)$$

provided

$$\sum_{i=1}^m \alpha_i y_i = 0 \qquad (12)$$

where $0 \leq \alpha_i \leq C$ denotes the Lagrangian multiplier. Support vectors of the pSVM correspond to data points for which the α values are nonzero. The Hessian matrix formed by $y_i y_j \emptyset(x_i x_j)$ of order (n x n), has a computational complexity of $O(n^2)$. The computational load for OVO ($O(2\frac{(k-1)n^2}{k})$) is lesser than that of OVA technique with ($O(k \, n^2)$, where *k* represents the number of classes with n data points. The ith SVM is trained with all examples in the ith class with positive labels and all other examples with negative labels. For each class j the SVM is trained in class j as positive and rest of the instances as negative.

A leave 20% out cross-validation is performed on the training data set. Optimum accuracy for the overall algorithm was obtained by finding the optimum values of C and γ using a grid search

procedure [28-29]. These optimum values of C and γ were fixed and used for prediction. Given a new input x, its class by was predicted by evaluation of the decision function given as

$$d = \text{sgn}\left(\sum_{k=1}^{n} y_n \alpha_k^{ij} \phi(x, x_k) + b^{ij}\right) \tag{13}$$

for

$$\alpha_k \geq 0.1 \tag{14}$$

Based on the above decision function, the algorithm discriminated between every pair of classes, and in selection of classes using a majority voting rule [30], meaning it selects a class with most winning two class decisions as given below.

$$\delta_p = \sum_i (\arg \max_j \sum I_{(d_{ij} > d_{ji})}) \tag{15}$$

where δ_p is a label predicting the ith class while the indicator function I represents a unity value if $d_{ij} > d_{ji}$. An SVM with larger margin and/or a smaller number of support vectors is expected to have better generalization performance [31].

VI.   **Experimental Results**

Data acquired from 164 subjects were used. Out of the 164 subjects (excluding those with nephortic syndrome, lymphangitis or deep vein thrombosis) undergoing ICVG, 79 subjects with various aortic and arterial disorders were considered for testing. The plot for cross validation accuracy against the penalty parameter C is plotted for different values of γ in Fig. 7.
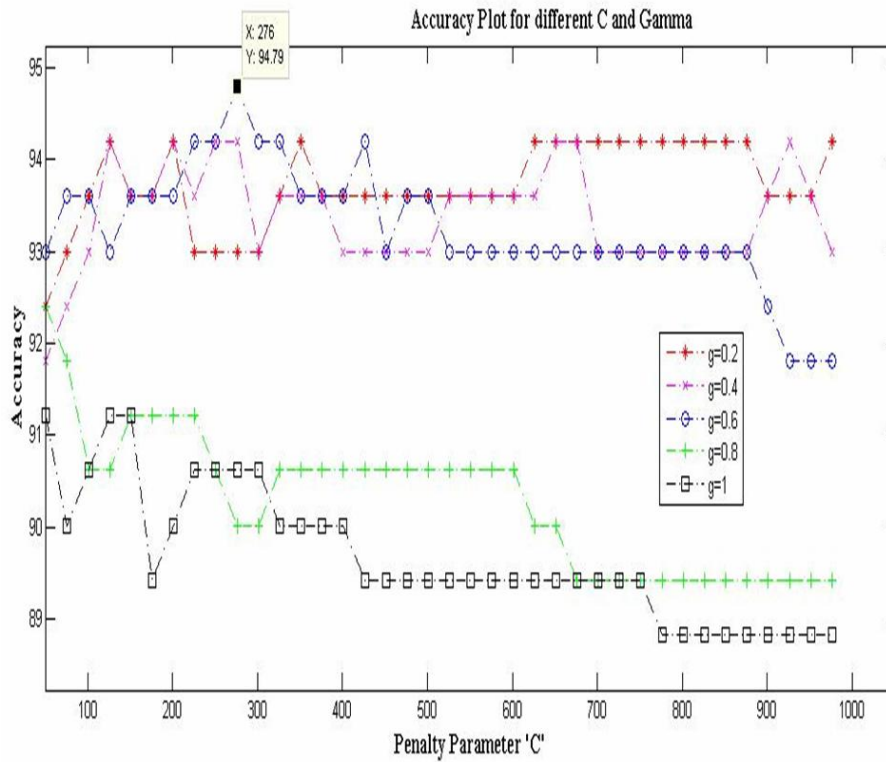

Figure 7: Cross Validation Prediction

The value of the parameters C (276) and γ (0.2) are obtained by maximizing the cross validation prediction. The above values of C and γ provide the highest cross validation accuracies. The corresponding test accuracies obtained are shown in Table 8.

Table 8: Cross validation and classification accuracy for pSVM and weighted pSVM architectures.

Parameters	pSVM	Weighted pSVM
Cross validation accuracy (%)	94	94.79
Classification (Test) accuracy (%)	96.2	97.46

9

Figure 8 illustrates the ICVG waveform of subject SJB-30-M with diseases of the calf vessels. The required BFI and DPAT parameters at the four locations are extracted using impedance cardiovasograph. Table 9 illustrates these parameters which represent the input to the pSVM architectures. The predicted output of the weighted pSVM is observed in Table 10.
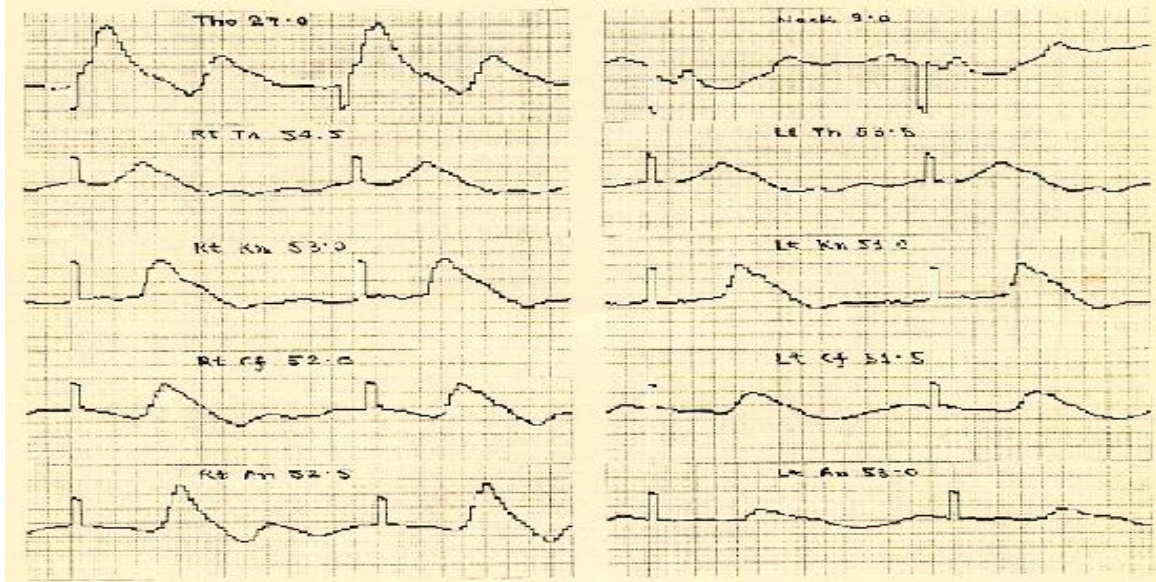

Figure 8: ICVG waveform recorded from a patient (SJB-30-M) with a disease of calf vessels.

Table 9: Extracted parameters from subject SJB-30-M

Location	Right Leg		Left Leg	
	BFI	DPAT	BFI	DPAT
Thigh	1.25	80	1.23	80
Knee	1.56	50	1.29	40
Calf	1.47	-	1.10	-
Ankle	1.61	20	0.70	50

Table 10: weighted pSVM prediction – SJB-30-M

Location	Right Leg	Left Leg
Thigh	I	I
Knee	I	I
Calf	I	III
Ankle	I	V

Table 10 gives the diagnosis for subject SJB-30-M based on the weighted pSVM algorithm. Though there is a slight reduction in DPAT value of the ankle in the right leg, the same is ignored in the view of normal and consistent BFI values. There is a marginal decrease in the value of BFI at the calf and a further decrease in its value at the ankle in the left leg with a marginal increase in DPAT indicating presence of an occlusion at the calf in the left leg. Figure 9 depicts the angiographic correlation which agrees with the simulated results.

Arteriogram of the left leg reveals external iliac, common femoral, superficial and deep femoral arteries to be normal. The trifurcation of popliteal artery and proximal portions of anterior and posterior tibial and the common peroneal arteries are seen to be normal. Posterior tibial is seen up to the distal calf region and not seen at ankle or below ankle region. The anterior tibial and common paroneal are not seen below mid calf region. These observations validate the ICVG diagnosis in this patient.

Figure 9: Angiographic Correlation (Courtesy, J.J Hospital & BARC, Mumbai, India)

Table 11 shows the performance results of the weighted pSVM on a set of 79 subjects with different combinations of aortic, femoral and distal blocks. Tables 12 - 14 show examples of false positive and false negative diagnosis of the weighted pSVM.

Table 11: Performance of proposed weighted support vector algorithm (pSVM)

Diagnosis with proposed weighted pSVM	No. of Subjects	Angiographic Results
Normal subjects correctly classified.	8	TN 16
Normal subject Aroposed algorithm predicts a distal artery block in the right limb	1	TN 1 FP 1
Normal subject Algorithm predicts a block at the thigh level in the right limb	1	TN 1 FP 1
Femoral artery occlusion in both limbs with varying collateral status at calf and ankle.	7	TP 14
Femoral artery occlusion in left leg with collateral status at calf and ankle. Right Leg gives normal diagnosis.	6	TP 6 TN 6
Femoral block with collateral conditions at calf and a further block at ankle in both limbs.	2	TP 4
Femoral block in one limb with a further block above the ankle. Normal diagnosis in the other limb.	4	TP 4 TN 4
Femoral block in the affected limb with collateral circulation. Atherosclerotic affection of aorta in the other limb	6	TP 12
Atherosclerotic affection of arteries. However, for one patient, our algorithm predicts normal for both limbs.	5	TP 8 FN 2
Narrowing of the aorta which persists throughout. Block above ankle in other limb. Arteriographic findings revealed a slight narrowing in one patient.	5	TP 10
Block above ankle in one limb. Normal diagnosis of the other limb.	3	TP 3 TN 3
Block above the ankle in both the limbs.	2	TP 4
Co-arctation of aorta with collateral condition at knee, calf and ankle.	3	TP 6

Hemi Leriche's syndrome Diagnosis of the other limb is Normal.	5	TP 5 TN 5
Occlusion at aortic-iliac bifurcation.	5	TP 10
Hemi Leriche's syndrome with collateral status at distal locations Narrowing detected in the other limb.	3	TP 6
Hemi Leriche's syndrome with a Further Block at ankle. Normal diagnosis of the other limb	2	TP 2 TN 2

TP: True Positive   TN: True Negative   FP: False Positive   FN: False Negative

Table 12: False Positive diagnosis by the weighted pSVM

Location	Right Leg		Left Leg	
	BFI	DPAT	BFI	DPAT
Thigh	0.86	80	0.95	60
Knee	1.26	30	0.58	30
Calf	1.25	00	1.47	00
Ankle	1.27	30	1.46	50

The case detected as False Positive is of a 56 year female as analyzed in Table 12. The support vector algorithm predicts a 'block' at the thigh level followed by 'good collaterals' at the knee, calf and ankle locations for the left limb while providing diagnosis for the other as 'normal'. Angiogram of the patient however shows normal blood circulation in both the limbs. There is an inconsistency in the data of the left leg which was not recognized by the algorithm.

Table 13: False Positive diagnosis by the weighted pSVM

Location	Right Leg		Left Leg	
	BFI	DPAT	BFI	DPAT
Thigh	0.75	70	0.73	70
Knee	1.37	30	1.21	50
Calf	1.23	-	1.33	-
Ankle	1.22	50	1.26	30

The case is of 25 year old male. Angiogram of the patient shows no significant arterial occlusion in the right limb. Our algorithm predicts a 'BLOCK' at the distal location in the right leg and a normal prediction for the left.

Table 14: False Negative diagnosis by weighted pSVM

Location	Right Leg		Left Leg	
	BFI	DPAT	BFI	DPAT
Thigh	1.03	50	0.98	60
Knee	1.09	30	0.83	30
Calf	1.03	-	1.07	-
Ankle	0.85	30	0.82	30

The above is a case of 60 year old male with pain in the right leg and an inability to walk for a long time. Digital angiogram in the patient shows tapered narrowing of both the subclavian arteries; however the algorithm predicts 'normal' diagnoses in both the limbs.

Table 15 provides the confusion matrix for the weighted pSVM architecture.

Table 15: Confusion Matrix for the weighted pSVM architecture

I	244	0	2	1	2	1	0	97.6%
	38.6%	0.0%	0.3%	0.2%	0.3%	0.2%	0.0%	2.4%
II	7	153	0	0	0	0	0	95.6%
	1.1%	24.2%	0.0%	0.0%	0.0%	0.0%	0.0%	4.4%
III	0	0	78	0	0	0	0	100%
	0.0%	0.0%	12.3%	0.0%	0.0%	0.0%	0.0%	0%
IV	0	0	0	40	2	0	0	95.2%
	0.0%	0.0%	0.0%	6.3%	0.2%	0.0%	0.0%	4.8%
V	0	0	0	0	42	0	0	100%
	0.0%	0.0%	0.0%	0.0%	6.6%	0.0%	0.0%	0%
VI	0	0	0	0	1	43	4	97.7%
	0.0%	0.0%	0.0%	0.0%	0.0%	6.8%	0.6%	2.3%
VII	0	0	0	0	0	0	16	100%
	0.0%	0.0%	0.0%	0.0%	0.0%	0.0%	2.5%	0%
TP	97.2%	100%	97.5%	97.6%	89.4%	97.7%	100%	97.5%
FN	2.8%	0%	2.5%	2.4%	10.6%	2.3%	0%	2.5%
Class	I	II	III	IV	V	VI	VII	TN FP

Output Class

Target Class

The coefficient of confusion is calculated as

$$c = \frac{\text{Number of misclassifications}}{\text{Total number of classifications}} = 0.0253 \tag{16}$$

Table 16 performs the ROC analysis for the weighted pSVM.

Table 16: ROC Analysis of weighted multiclass pSVM

Disease					
Test	Present	n	Absent	n	Total
Positive	True Positive (TP)	116 *(a)*	False Positive (FP)	2 *(c)*	118 *(a + c)*
Negative	False Negative (FN)	2 *(b)*	True Negative (TN)	38 *(d)*	40 *(b + d)*
Total	--	118 *(a + b)*	--	*40 (c + d)*	158

The ROC curves for non-weighted and weighted pSVM are as shown in Figure 10 (A) and 10 (B) respectively.

The performance of the multiclass weighted pSVM is compared against the Elman and PCA based backpropagation architectures in shown in Table 17. Backpropagation and PCA based backpropagation algorithms were implemented by the authors in [32] with the same plethysmographic data set.

Fig 10 (A): ROC-non-weighted pSVMs

Fig 10 (B): ROC-weighted pSVMs
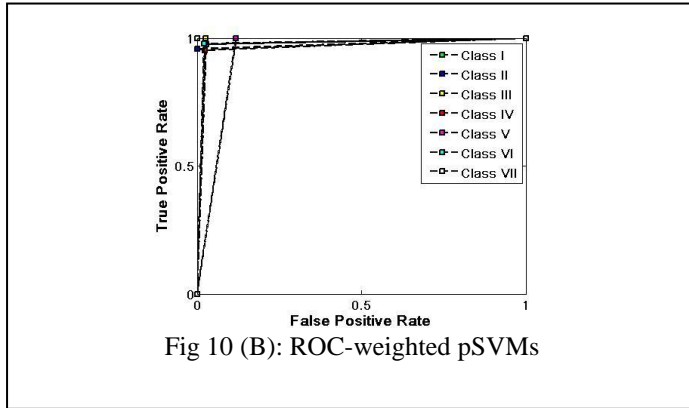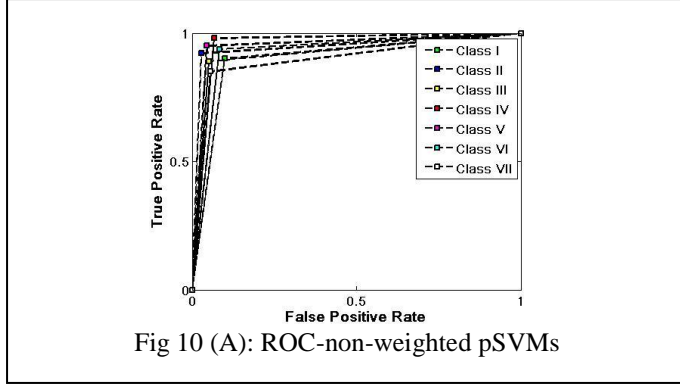
Using the confusion matrices, benchmark parameters were evaluated for the non-weighted and the weighted support vector multiclass pSVMs. While the other parameters have standard definitions, the F- score is defined as the harmonic mean between specificity and positive predictive value, and Matthews Correlation Coefficient (MCC) is defined as

$$MCC = \frac{TP*TN - FP*FN}{\sqrt{(TP+FN)(TN+FP)(TP+FP)(TN+FN)}}$$ (17)

Table 17: Performance comparison of proposed and existing architectures

Confusion Parameters	Backpropagation	PCA based backpropagation	Non-weighted pSVM	Weighted pSVM
Accuracy (%)	91.4	96.09	96.2	97.46
Precision (%)	94.19	98.85	98.29	98.3
Sensitivity (%)	93.1	95.5	96.63	98.3
Specificity (%)	87.8	97.36	94.8	95
F-score (%)	93.69	97.46	96.51	96.62
Negative Predictive Value (%)	85.71	90.24	90.24	95
Positive Likelihood Ratio	7.6311	36.31	18.58	19.66
Negative Likelihood Ratio	7.858	4.622	3.55	1.78
MCC	0.804	0.9098	0.90	0.933

Proposed weighted pSVM performs better than PCA based backpropagation and non-weighted pSVMs. A reduction of about 2% in the specificity (ability to identify the negative results) was compensated well by a

5% increase in the negative predictive value. The positive likelihood ratio greater than 10 significantly increases the likelihood that the subject is suffering from the disease if the diagnosis is positive as predicted by PCA based backpropagation and weighted and non-weighted pSVMs. However 60% reduction in the negative likelihood ratio due to a higher number of true negatives (subject is not affected with the disease when diagnosis is negative) as compared with other mentioned architectures is a significant contribution of the weighted pSVMs in the diagnosis of arterial occlusive diseases. In addition the highest MCC, a noteworthy parameter for multiclass comparison, exhibited by weighted pSVM substantiates this claim.

Conclusion

ICVG is used for diagnosis and early recognition of arteriosclerosis, chronic and/or acute arterial vascular diseases, and functional circulatory disturbances. It helps in estimating impact of pharmaceuticals on a vascular system. With the aid of an improved machine learning algorithms it enhances its utility to guide a clinician and aids a doctor in diagnostics.

A weighted pSVM architecture based method was proposed. The proposed method provides better accuracy and sensitivity than PCA based backpropagation and non weighted pSVM architectures. The significant contribution of the weighted pSVM method is the reduction of the negative likelihood ratio by over 60% and increase in the negative predictive value by more than 5%. The proposed method has more significance in case of tradeoff between sensitivity and specificity. A positive likelihood ratio of over 10 provided a large and conclusive increase in the likelihood of a disease, and it was supported with multiclass performance characteristic with Matthews correlation coefficient of 0.933.

The machine interpretation of the haemodynamic parameters, as proposed, may aid in proliferation of medical access to more persons.

References

[1]. G.D. Jindal, T.S. Ananthakrishnan and S. K. Kataria, "An introduction to impedance cardiovasography", Proc. Symposium on Biomedical Engineering and Nuclear Medicine (SBME-NM), Bhabha Atomic Research Centre, Mumbai, E /003, 2001.

[2] G. D. Jindal, T. S. Ananthakrishnan, S. K. Kataria, "Electrical impedance and photo plethysmography for medical applications", Proc. Symposium on Biomedical Engineering and Nuclear Medicine (SBME-NM), Bhabha Atomic Research Centre, Mumbai, E /025, pp.134-138, Microfiche 2005/60371 (Q)2005.

[3] J. C. Golden, D. S. Miles, "Assessment of peripheral haemodynamic using impedance plethysmography", Physical Therapy, vol. 66 (10), pp. 1544-1547, Oct. 1986.

[4] S. N. Mohapatra, A. M. Helena, "Measurement of peripheral blood flow by electrical Impedance technique", Journal of Med. Engg. & Tech., vol. 3 (3), pp. 132-137, 1979.

[5] C Corciova, R. Ciorap, D. Zaharia, D Matei, "On using impedance plethysmography for estimation of blood flow", Medical Measurements and Applications Proceedings (MeMeA), 2011 IEEE International Workshop on, pp.84-87, May 2011.

[6] C. Corciova, R. Ciorap, D. Zaharia, D. Matei, "Hemodynamic monitoring using peripheral impedance plethysmography", Advanced Topics in Electrical Engineering (ATEE), 7th International Symposium on, pp.1-4, May 2011.

[7] C. H. Lin, "Assessment of bilateral photoplethysmography for lower limb peripheral vascular occlusive disease using color relation analysis classifier", Comput. Methods Prog. Biomed, vol. 103 (3) pp. 121-131, 2011.

[8] R. D. Hull, G. E. Raskob, C. J. Carter, "Serial impedance plethysmography in pregnant patients with clinically suspected deep-vein thrombosis, clinical validity of negative findings", Annals of Internal Medicine, vol. 112 (9), pp. 663-667, 1990.

[9] J. J. Wang, W. C. Hu, T. Kao, C. Peng Liu, Shih-Kai Lin, "Development of forearm impedance plethysmography for the minimally invasive monitoring of cardiac pumping function", Journal of Biomedical Science and Engineering, vol. 4 (6), pp. 122-129, 2011.

[10] Peripheral Pulse Analyzer, Internet: Available from:http://www. [Last Accessed June 2012] larsentoubro.com/lntcorporate/uploads/product/Nivomon.pdf

[11] J. Webster, T. M. Ravi Shankar, S.Y. Shao, "The contribution of vessel volume change and blood resistivity change to the electrical impedance pulse", IEEE Transactions on Biomedical Engineering, vol. BME-32, (3), pp 192-198, March, 1985.

[12] B. H. Brown, W. I. J. Pryce, R. G. Clarke, "Impedance plethysmography: Can it measure changes in limb blood flow", Medical & Biological Engg, pp 674-681, Sept., 1975.

[13] W. G. Kubicek, J. Kottke, M. U. Ramos, R.P. Patterson, D.A. Witsoe, J.W. Labree, "The Minnesota impedance cardiograph- theory and applications", Biomed Engg. vol. 9, pp. 410-416, September 1974.

[14] T. S. Ananthakrishnan, G. D. Jindal, V. Sinha, R. K Jain, S. K. Kataria, A. K Deshpande, "Clinical validation of software for a versatile variability analyzer: Assessment of autonomic function, vol. 32 (3), pp. 97-102, 2007.

[15] G. D. Jindal, J. P. Babu, "Calibration of dZ/dt in impedance plethysmography", Med. & Bio. Engg. & Comput., vol. 23, pp 279-280, 1985.

[16] A. C. Bhuta, J. P. Babu, G. B. Parulkar, "Technical aspects of impedance plethysmography", Journal of Post Graduate Medicine, vol. 36 2, pp. 64-70, 1990.

[17] G. D. Jindal, J. P. Babu, S. N. Nerurkar, M. D. Kelkar, A. K. Deshpande, "Corrected formula for estimating peripheral blood flow by impedance plethysmography", Med. Bio.Engg. Comput., vol. 32, pp.625-631, 1994.

[18] S. Karamchandani, M. Y. Dixit, R. K. Jain, M. Bhowmick, "Application of neural networks in the interpretation of impedance Cardiovasograms for the diagnoses of peripheral vascular diseases", Conf Proc IEEE Engg. Med. Biol. Soc, vol. 7, pp.7537-40, 2005.

[19] J. P. Babu, T. S. Anathakrishnan, S. Mandlik, and G. D. Jindal, "PC based impedance cardio-vasography", SBME-NM, BARC, 2000.

[20] O. Ozcan, S. Mustafa, D. A. Duran, G. Bilal, A. Omer, C. Gokhan, T. Serkan, A. Dursun, B. Yucel, S. Hatice, "Do collaterals affect heart rate variability in patients with acute myocardial infarction?", Coronary Artery Disease, vol. 15, (7), pp 405-411, Nov. 2004.

[21] R. D. Hill, R. B. Smith, "Examination of the extremities: Pulses, Bruits, and Phlebitis", Clinical Methods, pp 148-153, 1990.

[22] C-C. Chang, C-Jen Lin, LIBSVM: a library for support vector machines, 2001.

[23] O Ivanciuc, "Applications of support vector machines in chemistry", Reviews in Computational Chemistry, vol. 23, Wiley-VCH, Weinheim, pp 291-400, 2007.

[24] C. Hsu, C. Lin, "A comparison of methods for multi-class support vector machines", IEEE Transactions on Neural Networks, vol. 13, pp.415-425, 2002.

[25] Yi-Min Huang , Shu-xin Du, "Weighted support vector machine for classification with uneven training class sizes", Proceedings of the Fourth International Conference on Machine Learning and Cybernetics, Guangzhou, pp 4365-4369, Aug. 2005.

[26] S. S. Keerthi, C.-J. Lin, "Asymptotic behaviors of support vector machines with Gaussian kernel", Neural Computation, vol. 15, (7), pp 1667-1689, 2003.

[27] H.T. Lin, C.J. Lin,"A study on Sigmoid kernels for SVM and the training of non-PSD kernels by SMO-type Methods", Technical Report. National Taiwan University, March, 2003.

[28] F. F. Chamasemani, Y.P.Singh, "Multiclass Support Vector Machine (SVM) classifiers - An application in hypothyroid detection and classification", IEEE Bio-Inspired Computing Theories and Applications (BIC-TA), Sixth International Conference on, pp. 351-356, 2011.

[29] C. Hsu, C. Chang, C. Lin, "A practical guide to support vector classification", http:///www.csie.ntu.edu.tw, May, 2009.

[30] T. F. Wu, C. J. Lin, R. C. Weng, "Probability estimates for multiclass classification by pairwise coupling", Journal of Machine Learning Research, vol. 5, pp 975-1005, 2004.

[31] Yiguang Liu, Zhisheng You, Liping Cao, "A novel and quick SVM-based multiclass classifier", Pattern Recognition vol. 39, pp. 2258 – 2264, Elsevier, 2006.

[32] S.Karamchandani, U.B.Desai, S.N.Merchant, "Principal component analysis Based backpropagation algorithm for diagnosis of peripheral arterial occlusive diseases", Proc. Canadian Conference on Electrical and Computer Engineering, 2009.